Applied Catalysis B: Environmental 257 (2019) 117917

Contents lists available at ScienceDirect

Applied Catalysis B: Environmental

journal homepage: www.elsevier.com/locate/apcatb

# Enhanced electrocatalytic performance triggered by atomically bridged boron nitride between palladium nanoparticles and carbon fibers in gas-diffusion electrodes

Matthieu Weber[a], Nazym Tuleushova[a], Joelle Zgheib[a], Cassandre Lamboux[a], Igor Iatsunskyi[b], Emerson Coy[b], Valerie Flaud[c], Sophie Tingry[a], David Cornu[a], Philippe Miele[a,d], Mikhael Bechelany*[,a], Yaovi Holade*[,a]

[a] Institut Européen des Membranes, IEM–UMR 5635, ENSCM, CNRS, Univ Montpellier, Montpellier, France
[b] NanoBioMedical Centre, Adam Mickiewicz University, Wszechnicy Piastowskiej 3, 61-614, Poznan, Poland
[c] Institut Charles Gerhardt Montpellier, UMR5253, ENSCM, CNRS, Univ Montpellier, Montpellier, France
[d] Institut Universitaire de France, 1 rue Descartes, 75231, Paris, France

ARTICLE INFO

*Keywords:*
Atomic layer deposition
Boron nitride
Palladium nanoparticles
Oxygen reduction reaction
Ethanol electrooxidation reaction

ABSTRACT

Significant reduction of the amount of precious metals in catalysts is a major challenge. We report the synthesis of high-performance carbon paper-boron nitride-palladium (CP-BN-Pd) electrocatalytic electrodes. The nanocatalysts consist of Pd nanoparticles of 5 nm supported on an ultrathin BN film prepared by atomic layer deposition (ALD), covering the microfibers of gas-diffusion electrodes (GDL). These electrodes present significantly enhanced electrocatalytic performance towards oxygen reduction (ORR) and C2 alcohols oxidation reactions and outperform the reported data for those alcohols in alkaline media, reaching a peak current of 17 amps/$mg_{Pd}$ in 1 M NaOH + 1 M ethanol. The ageing tests reveal excellent stability of the electrochemically active surface area even after 1000 cycles, and the ethanol oxidation activity shows negligible decay of 1% whereas commercial Pd/C show prominent decay of 44%. The use of this heterogeneous active interface opens a new route for the development of efficient and low-metal content nanocatalysts.

## 1. Introduction

The electrochemical energy conversion and storage devices of fuel cells (FCs) and electrolysis cells (ECs) are rapidly growing as part of X-to-Power and Power-to-X energy transition scenarios [1–3]. The systems utilizing anion exchange membrane (AEM) have emerged in recent years as possible low-cost energy devices resulting from the fact that alkaline media overcomes the existing cost barriers of proton exchange membrane (PEM) [4–8]. Oxygen reduction reaction (ORR) is the key cathode reaction for both FCs and metal-air batteries. The anode oxidation of biomass-based compounds such as ethanol and glycerol (less toxic, cheaper, easier to store and handle) emerges as a sustainable and attractive alternative in FCs to produce electricity and ECs for low-energy consumption $H_2$ production [9–12]. The sluggishness of the electrochemical kinetics of both cathode and anode reactions is so important that platinum group metals (PGM) are considered to be the essential cornerstone catalytic species. The diminution of the loadings of these precious metals (below 0.1 mg $cm^{-2}$) while keeping or even increasing performance is a key challenge [6,13]. To date, almost all the synthesis routes focus on the decomposition of precursors in the presence of surfactants or stabilizers to engineer catalytic materials with tunable surface structure and composition, ranging from nanocages, nanowires, nanoframes, nanosponges, mesoporous materials, nanoalloys to highly-faceted materials [2,3,9,14]. Hence, the nanoparticles (NPs) do not take the advantage of the metal-support interaction [15,16] and have to be stabilized in a liquid or dispersed in a powder before using a binder such as Nafion for immobilization on a substrate (mostly glassy carbon) during various post-synthesis steps. While the use of such ionomer contributes to the proton transport, the process adds a layer of complexity to the fabrication process, the isolation of some NPs is common and the degradation during the long-term catalysis results in the undesired loss of active sites and subsequent decrease in catalytic performance [17]. In addition, those methods result in high loadings of precious metals. To avoid the need to collect and immobilize NPs after their synthesis, the ideal solution is to directly prepare them on their own support of FCs and ECs that is the three-

* Corresponding authors.
*E-mail addresses:* mikhael.bechelany@umontpellier.fr (M. Bechelany), yaovi.holade@enscm.fr (Y. Holade).

https://doi.org/10.1016/j.apcatb.2019.117917
Received 28 March 2019; Received in revised form 28 June 2019; Accepted 4 July 2019
Available online 05 July 2019
0926-3373/ 

dimensional (3D) gas-diffusion layer electrodes (GDL) [18]. Among the solutions for the advantageous direct growth of NPs on GDL electrodes, atomic layer deposition (ALD) appears as a promising route, as materials can be prepared in a layer-by-layer basis at the atomic-level thickness control as well as an excellent uniformity and conformality over the substrate surface, which makes this technique applied in a myriad of applications [19–27].

Using ALD to elaborate electrocatalysts enables to maximize the metal-support interaction and impact the electronic properties of active sites, thus changing the adsorption strength of reactants and intermediates, resulting in improved reactivity and stability [15,16]. Assaud et al. [21,22] have shown that, in alkaline media, the electrochemically active surface area (ECSA) and ethanol's electrocatalysis of ALD-synthesized Pd NPs is much improved. Recently, our group has shown that the increase of the glycerol activity by an order of magnitude in comparison to the Pd/C reference is reachable by decorating microfibers of a carbon felt electrode with Pd NPs of 4–6 nm at the reduced loading of 96 $\mu g_{Pd}\,cm^{-2}$ [23]. It has been reported that boron nitride (BN) film enables improving the efficiency of number of heterogeneous catalysis reactions [28–32] substantiated by theoretical studies [28,33,34]. However, to the best of our knowledge, there is no report in the literature on the performance of ALD grown Pd NPs on BN surfaces, despite the great potential of this combination. It is also missing the electrochemical properties of BN-Pd coated large surfaces of GDL such as those used in energy technologies. Conclusively, a fundamental knowledge is missing about the electrocatalytic properties of Pd NPs supported on GDL electrodes through a nano-bridge of BN.

To address all those challenges and establish a performance trend, we report herein the design, synthesis and assessment of the electrocatalytic properties of those new classes of ALD-grown GDL-BN-Pd freestanding electrodes with tunable BN's thickness towards four model-reactions of $Fe(CN)_6^{3-/4-}$ redox probe, ORR, ethanol and ethylene glycol oxidation. When BN bridges Pd NPs and carbon microfibers, the resulting electrode of 5 $\mu g_{Pd}\,cm^{-2}$ showed surprisingly high electrochemical kinetics for all tested reactions. The catalysts also exhibited excellent durability results. It is expected that the developed strategy can be readily extended to other type of low metal content catalysts thus re-enforcing the possible widespread deployment of ALD-based materials in heterogeneous catalysis.

## 2. Experimental

### 2.1. Reagents and materials

GDL-based carbon paper (CP, AvCarb MGL190, 190 µm thickness, Fuel Cell Earth LLC), ethanol (EtOH, VWR, 100%), sodium hydroxide (NaOH, Prolabo, 99%) and potassium hydroxide (KOH, Prolabo, 85%) were used as received. Isopropanol (ACS reagent, ≥99.8%), palladium hexafluoroacetylacetonate ($Pd(hfac)_2$, 95%, potassium nitrate ($KNO_3$, 99%), Nafion® suspension (5 wt%), ethylene glycol (EG, ≥99%), boron tribromide ($BBr_3$, 99.9%), formalin (37 wt.% in $H_2O$, contains 10–15% methanol as stabilizer) and potassium hexacyanoferrate ($K_3[Fe(CN)_6]$, ≥99.0%) were purchased from Sigma-Aldrich and used as received. Gases ($O_2$, $N_2$, Ar, $NH_3$) and water (Milli-Q Millipore, 18.2 MΩ cm at 20 °C) were ultrapure. Commercial catalyst is Pd/C (20 wt%, 3–4 nm, Premetek Co., USA).

### 2.2. Nanocatalysts synthesis by ALD

The GDL substrates were 5 cm high, 1 cm width, and 0.19 mm thickness. All depositions have been carried out in a low pressure hot-wall ALD reactor [35]. The BN process was based on $BBr_3$ precursor and $NH_3$ as co-reactant. Both $BBr_3$ and $NH_3$ lines were directly connected to the reactor through gate valves and heated at 100 °C to avoid condensation. The deposition chamber was set at 750 °C. The typical ALD cycle consists of 0.1 s pulse of $BBr_3$, 5 s exposure, and 15 s purge, followed by a 3 s pulse of $NH_3$, 5 s exposure and 15 s purge with Ar. The as-fabricated samples with different thicknesses of BN are referred to as CP-BN*x* (*x* = 10, 20, 40 Å). The Pd process was based on ($Pd(hfac)_2$) and formalin as co-reactant. The formalin was kept at room temperature and the $Pd(hfac)_2$ was heated at 70 °C to have sufficient vapor pressure. The lines were heated at 100 °C to avoid any condensation and the deposition chamber was set at 220 °C. The typical ALD cycle consists of 5 s pulse of $Pd(hfac)_2$, 15 s exposure, and 20 s purge, followed by a 1 s pulse of formalin, 15 s exposure and 60 s purge with Ar. The synthesized electrodes are labeled to as CP-Pd or CP-BN-Pd.

### 2.3. Physicochemical characterization

Transmission electron microscopy (TEM) was performed using JEOL 2200FS (200 kV) and JEOL ARM-200 F (200 kV). Inductively coupled plasma optical emission spectrometry (ICP-OES) analysis was performed on a spectrometer Optima 2000 DV (PerkinElmer). X-ray photoelectron spectroscopy (XPS) was fulfilled on an ESCALAB 250 spectrometer (Thermo Electron, monochromatic radiation source Al Kα = 1486.6 eV). Survey spectra were recorded at a step of 1 eV (transition energy: 150 eV) and high-resolution spectra were recorded at a step of 0.1 eV (transition energy: 20 eV). The measurement of binding energy (BE) was corrected on the basis of the energy of C1s at 284.4 eV, and the quantification was carried out from the corresponding XPS peak area after correction with a suitable sensitivity factor.

### 2.4. Electrochemical and catalytic measurements

The half-cell electrochemistry was studied in a conventional three-electrode cell. Ag/AgCl/KCl (3 M) was used as reference electrode and was separated from the solution by a Haber-Luggin capillary tip. However, control experiments in alkaline solution were performed using Hg/HgO/Na(K)OH. Most of potentials were scaled versus the reversible hydrogen electrode (RHE) according to the calibration relationship $E$(V vs RHE) = $E$(V vs Ag/AgCl) + $\Delta E$, with $\Delta E$ = 0.959 V (0.1 M NaOH) and 1.010 V (1 M NaOH). The calibrating with respect to RHE was performed in the high-purity $H_2$-saturated electrolyte (Fig. S1). A slab of glassy carbon (12.4 $cm^2$) was used as counter electrode. The working electrode consists of a CP-based electrode cut into L-shape of 1 cm high and 0.5 cm width, leading to an estimated area of 1 $cm^2$ and enough space on the top for electrical wiring with gold. The catalytic ink preparation for the commercial material follows standard procedures. Typically, 180 µL of isopropanol and 20 µL of Nafion® suspension were ultrasonically mixed. Then, 2.4 mg of Pd/C powder was added. Finally, 7 µL of the homogeneous ink was drop-casted onto each face of a bare L-shape CP electrode of 1 cm high and 0.5 cm width and dried at room temperature under $N_2$ flow. The Pd value assessed by ICP being 23.5 wt.%, the loading is 39 $\mu g_{Pd}\,cm^{-2}$. Electrochemical characterization by the redox probe $Fe(CN)_6^{3-}/Fe(CN)_6^{4-}$ was performed in 1 M $KNO_3$. Given the Pd NPs ability to absorb hydrogen into their crystal lattice, we used the PdO reduction peak (Fig. S2) by considering a monolayer charge density of 424 µC $cm^{-2}$ [36,37]. EtOH and EG oxidation reactions were investigated by the methods of cyclic voltammetry (CV), chronoamperometry (CA) and potentiostatic electrochemical impedance spectroscopy (EIS). ORR polarization curves were obtained with $O_2$-saturated electrolyte. Since the as-synthesized materials are freestanding (in the form of a sheet), the classical rotating (ring)-disk electrode R(R)DE setup could not be used to routinely overcome the diffusion process setup and run ORR under different rotation speeds. The polarization was thus collected by gently stirring the solution. Preliminary EIS was performed at OrigaStat OGS100 potentiostat (Origalys) scanning frequencies from 1 kHz to 25 mHz (10 mV amplitude). Then, SP150 potentiostat (Biologic Science Instruments) was used for frequencies of 200 kHz to 25 mHz (10 mV amplitude). All the voltammograms are iR-free, *i.e.*, corrected by the "potential drop" between the working and reference electrodes according

to the relationship $E_{real} = E_{applied} - R_{\Omega} \times I$. $R_{\Omega}$ is obtained by EIS at the intersection between the Nyquist curve and *x*-axis at high frequencies, herein $R_{\Omega}$ ~20 Ω in 0.1 M NaOH and ~3 Ω in 1 M NaOH (for 1 $cm^2$ working electrode).

## 3. Results and discussion

### 3.1. Electrochemical performance of the developed BN nanolayers at the surface of a gas-diffusion electrode

In the following sections, the overall process of ALD assisted fabrication of the electrode materials and electrochemical tests have been validated by running more than three times the studies and the conclusion is that the process is reproducible (different samples and different operators). To determine if the surface of CP would be favorable to the deposition of a layer of BN and Pd NPs or not, we first carried out a systematic physicochemical investigation. We especially aimed to study the hydrophobic/hydrophilic character, as that is the presumed starting point to have a good wettability, a prerequisite for use in electrocatalysis in aqueous media. Indeed, in some cases, it is necessary to perform an activation step before NPs deposition or obtaining significant electrocatalysis [23]. As-shown in Fig. 1a, the pristine CP electrode (190 µm thickness) is composed of ~7 µm diameter microfibers, which means than the entire electrode could be described as a stack of 190/7 = 27 layers of fibers. XPS survey (Fig. 1b) shows O and C signals and the high resolution spectrum of the C1s core level (Fig. 1c) demonstrates the presence of oxygenated species on the surface, thus making the surface hydrophilic. Performed water-contact angle-measurements have upheld the wettability of the material. Those results confirm that CP can be used in aqueous media without any further pretreatment steps.

To gain a deep understanding on the effects of B, N co-modification on the performance, we first prepared a series of CP-based materials by varying the BN atomic layer thickness. The optimized ALD process allows for the saturated growth of conformal BN films with a steady-state growth of ~0.8 Å/cycle with no visible nucleation delay [35,38]. Several analytical methods have been used to characterize the films, and the growth-per-cycle, C and O contents, roughness and mass density values are given in the Table S1. In the present study, we applied different cycles in order to coat the pristine CP substrate with an ultrathin film and referred to as CP-BN*x* (*x* = thickness in Å). Then, the samples were electrochemically probed in the presence of $Fe(CN)_6^{3-}$/$Fe(CN)_6^{4-}$ as the quasi-reversible redox probe, herein used to evaluate electrochemical kinetics. In order to provide a better qualitative and quantitative analysis of the electrochemical parameters, we used two different methods [39–42], namely the peak-to-peak separation ($\Delta E_p$) between the anodic and cathodic peaks on a CV and the EIS. The control experiments using a Pt RDE and the collected results are reported in Fig. S3-S6. Fig. 2a shows the steady-state profiles of CVs in the presence of the substrate while those recorded in the electrolyte are displayed within Fig. S7. The blank voltammograms indicate an increase of the capacitive current when BN thickness augments, which is in agreement with the presence of BN that is a lesser electron conductor than CP. However, we unexpectedly found from Fig. 2a that the introduction of BN atomic layer increases significantly, from +20 to 70%, the peak current density associated to the oxidation and reduction waves assigned to $Fe(CN)_6^{4-}$ and $Fe(CN)_6^{3-}$, respectively. Please note that the background current is highly negligible (Fig. 2a versus Fig. S7). From the $\Delta E_p$ modeling curve of Fig. S6, we specifically determine the standard rate constant ($k^\circ$), charge transfer resistance ($R_{ct}$) and exchange current density. $k^\circ(10^{-3}$ cm $s^{-1}) = 1.7$, 2.0, 6.2, and 10.5 for CP, CP-BN10, CP-BN20, and CP-BN40, respectively (Table S2). Those data correspond to a significant enhancement of the electrochemical kinetics by factors of 1.2–6.3 upon the deposition of BN. It features the ability to regulate the kinetics by the means of BN's ALD. Specifically, the trend can be translated to as a decrease of $R_{ct}$. Fig. 2b shows EIS data at open circuit potential (OCP) and the corresponding $R_{ct}$ and $k^\circ$ determined by using $R_{\Omega} + Q_{CPE}//(R_{ct} + W)$ as a representative equivalent electrical circuit (EEC) wherein *W* is the Warburg impedance (to model the mass transfer, *i.e.*, diffusion) and $Q_{CPE}$ is the constant phase element (to

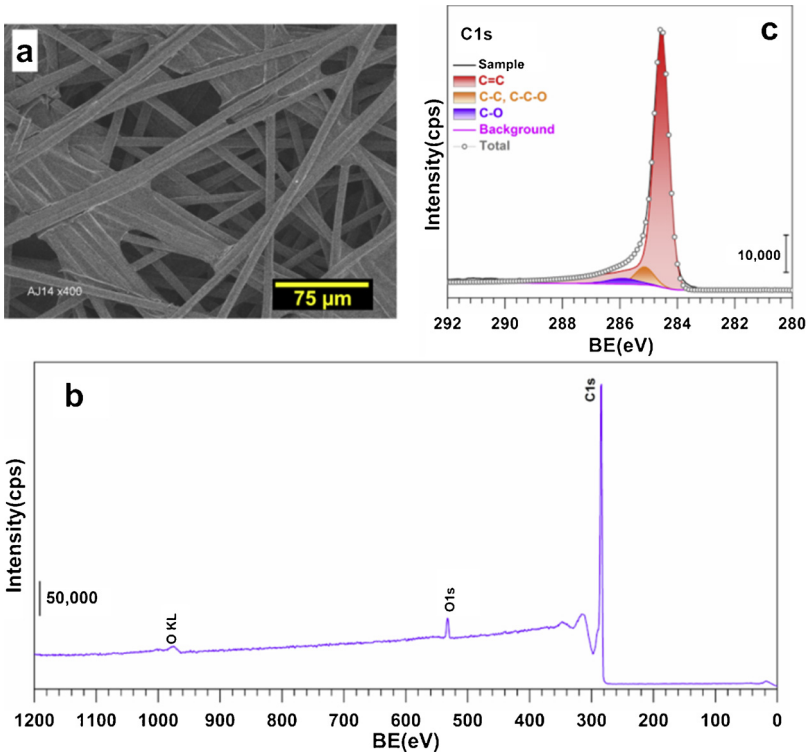


**Fig. 1.** (a) SEM image of the bare CP electrode. (b) Survey XPS spectra of the CP electrode. (c) High-resolution XPS spectrum of the C1s core level for the bare CP electrode.

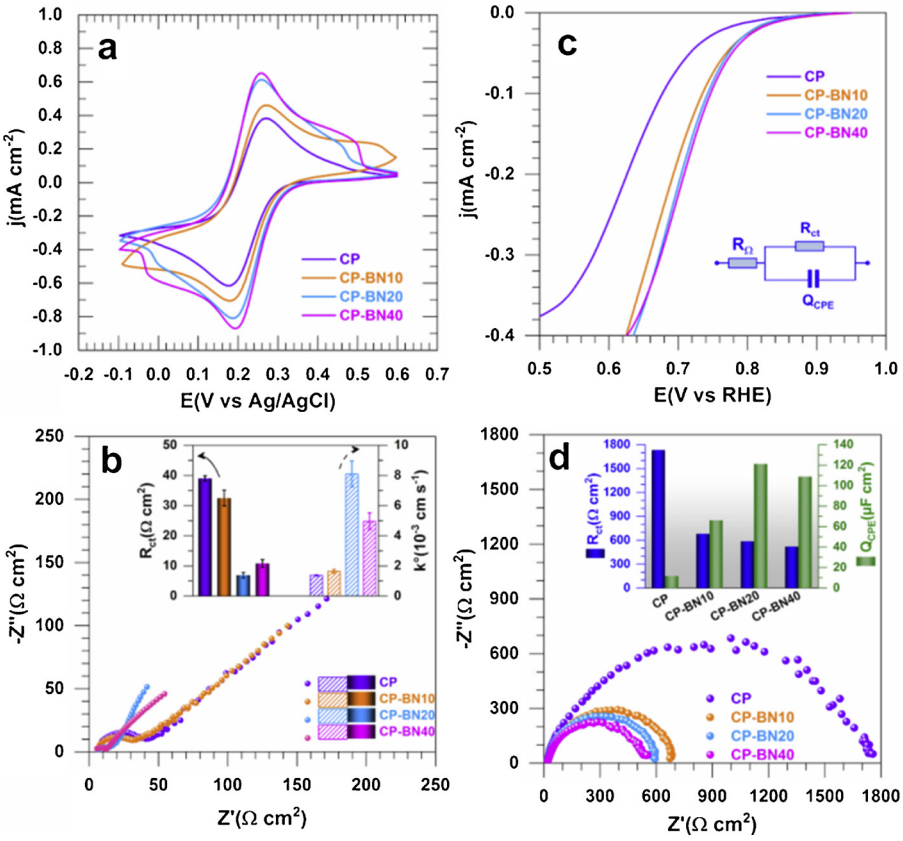


**Fig. 2.** (a) iR-free steady-state CVs recorded at 10 mV $s^{-1}$ for pristine CP and as-fabricated electrodes in 10 mM $K_3[Fe(CN)_6]$ + 1 M $KNO_3$. (b) Complex-plane Nyquist impedance plots at $E_{appl}$ (=OCP) = 0.3 V vs Ag/AgCl: the inset shows the fitted $R_{ct}$. (c) iR-free ORR LSVs recorded on pristine CP and as-fabricated CP-BN in $O_2$-saturated 0.1 M NaOH at 5 mV $s^{-1}$: the inset shows the used EEC for fitting. (d) Complex-plane Nyquist impedance plots at $E_{appl}$ = 0.81 V vs RHE in $O_2$-saturated 0.1 M NaOH: the inset shows the fitted $R_{ct}$ (left *Y*-axis) and $Q_{CPE}$ (right *Y*-axis). The temperature is 25 °C. Error bars represent one standard deviation ($n$ = 3).

model "imperfect" capacitors) [43,44]. This second method confirms the observed trend for the metrics of $R_{ct}$, $k^{\circ}$, and $j_0$. $R_{ct}$ (inversely proportional to $k^{\circ}$, thus $j_0$), is the ability of electron-transfer and the difficulty of an electrode reaction for driving larger current density with a less driving force [45]. For a given electrode, the bigger $R_{ct}$ is, the lower is the kinetic rate and lesser is the driving force. It can thus be concluded that the presence of BN improves the transfer of one electron from the catalytic surface to the reactant, while the reverse is true. With nearly one order of magnitude increase of $k^{\circ}$ for BN-modified CP, one can come up with a beneficial effect of the atomically bridged heteroatoms on the electrochemical kinetics of one electron-transfer process of a quasi-reversible [46,47].

The above outcomes demonstrate only our ability to regulate the kinetics of one electron-transfer process that is $Fe(CN)_6^{3-} + e^- = Fe(CN)_6^{4-}$. Suitability of modified electrodes for applications in heterogeneous electrocatalysis may require larger number of electrons. So, we next theorized a same trend for much higher number of electrons. To validate such hypothesis, we investigated ORR in alkaline media which is of paramount importance in electrochemical energy conversion and storage technologies. The performance in 0.1 M NaOH is displayed in Fig. 2c-d for LSVs and EIS at $E_{appl}$ = 0.81 V vs RHE. The inset shows the fitted EIS data by an EEC of $R_{\Omega}+Q_{CPE}//R_{ct}$ (extended data in Table S3). It should be noted that we firstly determined the depth of ORR by using our routine hydrogen peroxide method that combines chronoamperometry and UV–vis [48]. After chronoamperometry, samples are then acidified toward pH 3.5 ($pK_a(H_2O_2/HO_2^-)$ = 11.75, any produced $H_2O_2$ from the incomplete ORR is a form of $HO_2^-$), and the resulting $H_2O_2$ was quantified by spectrophotometry, using potassium titanium (IV) oxalate as a colored indicator via a calibration curve obtained from standard solutions. Then, the absorbance of the yellow pertitanic acid complex between $H_2O_2$ and potassium titanium oxalate in acidic solution is measured at $\lambda$ = 400 nm. We did not observe any significant amount of intermediate species for $E \geq$ 0.8 V vs RHE. Thus, it can be argued that ORR at the entire electrodes is a 4-electron process ($O_2 + 2H_2O + 4e^- \rightarrow 4OH^-$) so that kinetics parameters can be accurately well compared. Chen et al. [28] have shown that ORR starts at 0.8 V vs RHE for a catalytic ink of BN materials drop-casted onto RDE (by mixing catalytic powder, solvent and Nafion ionomer) in a 2-electron major process. The high selectivity observed on the present materials can be explained by synthesis procedure leading to surfaces that foster the perpendicular binding of $O_2$ and results in its cleavage. The polarization curves in Fig. 2c highlight a prominence shift of the potential towards higher potential, *i.e.*, lower overpotential. Similar improvement of the electrochemical performance of carbon substrates modified by B and N elements has been reported for other reactions and assigned to the heteroatom-carbon interface that acts as reactive sites [28,30–32,34,49–51]. From EIS data, the high activity originates from the decrease of $R_{ct}$, about 60–70% upon the deposition of BN layer, which accelerate the rate of the catalytic reaction. For a potential deployment as an ORR's cathode material for fuel cells or metal-air batteries purposes, the electrode should show large current density for potential higher than 0.8 V vs RHE. As the efficiency is below the threshold, the only possibility is its use as scaffolds for the deposition of ultra-low amount of active Pd metal, ideally lower than 50 μg $cm^{-2}$ [4,6,13].

### 3.2. Electrochemical probing and physicochemical characterization of Pd modified CP-based electrodes

Having demonstrated the ability to use ALD to grow BN nano-layers directly onto a GDL support, we sought to study the modification by electrocatalytic active Pd NPs more carefully. Indeed, the suitability of electrode materials for their application as cathodes may not require the presence of Pd, but for anode catalyst for fuel oxidation, the presence of those elements termed as PGMs is mandatory to achieve high current densities at lower overpotentials. Based on the previous results, we selected CP-BN20 for comparative studies with CP to fabricate by 100 cycles of Pd ALD, CP-Pd and CP-BN-Pd electrodes. Then, their

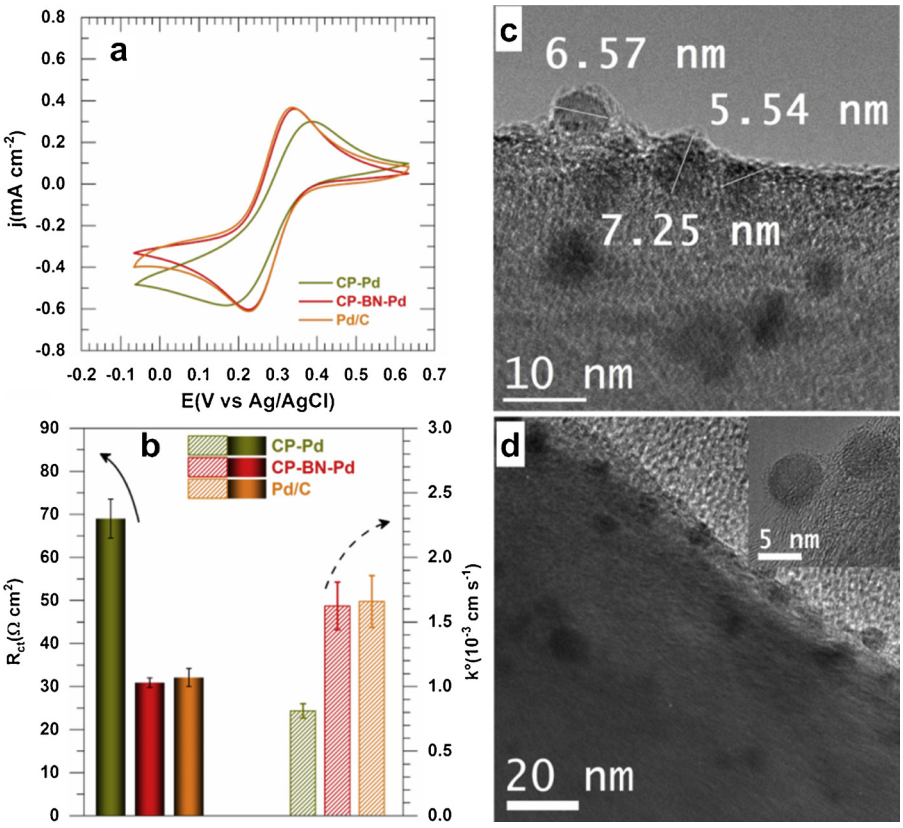


**Fig. 3.** (a) iR-free steady-state CVs recorded at 10 mV $s^{-1}$ in $N_2$-saturated 10 mM $K_3[Fe(CN)_6]$ + 1 M $KNO_3$: The temperature is 25 °C. (b) Extracted kinetics data of $R_{ct}$ (left *Y*-axis) and $k^\circ$ (right *Y*-axis) from EIS performed at $E_{appl}$ (≈ OCP) = 0.3 V vs Ag/AgCl. (c) TEM of CP-Pd. (d) TEM of CP-BN-Pd. Error bars represent one standard deviation ($n$ = 3).

electrochemical behaviors were confronted to the commercial Pd/C (20 wt.%, "C" denotes carbon Vulcan XC-72) presenting similar Pd NPs size (3–4 nm). Fig. 3a shows the profiles of the steady-state CVs in the presence of the redox probe, $Fe(CN)_6^{3-}/Fe(CN)_6^{4-}$. The extracted kinetics data of $k^\circ$, $R_{ct}$ and $j_0$ from the peak-to-peak separation method are gathered in Table S2 wherein $j^\circ$(mA $cm^{-2}$) is 0.3, 0.9 and 1.0 for CP-Pd, CP-BN-Pd and Pd/C, respectively. The values of $R_{ct}$ and $k^\circ$ extracted from the second method of EIS performed at $E_{appl}$(= OCP) = 0.3 V vs Ag/AgCl are shown in Fig. 3b and confirm the accelerated electrochemical kinetics when BN is intercalated between carbon surface and Pd NPs. The elementary analysis by ICP-OES shows that the Pd content in CP-Pd and CP-BN-Pd is about 30 and 5 µg $cm^{-2}$, respectively. Furthermore, it can be deduced from TEM images (for this purpose, single fiber was prepared) of Fig. 3c (CP-Pd) and 3d (CP-BN-Pd) that the Pd NPs are crystalline with a size distribution of 5 ± 2 nm. A deeper analysis indicates that the NPs of quasi-spherical shape are well dispersed all over the surface of the BN coated fibers with a longer distance between individual NPs. This enables to diminish the total amount of the precious metal. As the BN layer is turbostratic, the strength of interaction between the BN layer and the Pd clusters is difficult to determine. Many competing surface reactions occur during ALD, and these reactions are both very dynamic and complex. The initial growth of ALD of palladium at the BN surface is likely to start with the chemisorption reaction between the $Pd(hfac)_2$ precursor and the BH or NH groups present at the surface, resulting in the deposited Pd atoms and volatile H(hfac) species. The strength of the chemical bond between the Pd atoms and the BN surface can be determined by theoretical calculations. From theoretical studies carried out in the past, it has been found that in all cases, the B atom is closer than the N atom to the palladium surface, and the h-BN-palladium bonding energy is around 0.4 eV [52,53]. Taken together, those set of results demonstrate that the presence of a ~2 nm BN layer enables lowering significantly the loading of Pd while getting high electrochemical kinetics. The BN surface presents a certain number of atoms in direct contact with the palladium NPs, thus forming an atomically bridged region between the carbon and the noble metal material. The electrons are able to readily cross this thin BN nanolayer bridge to reach the carbon fiber, and this bridged region is likely to explain the superior electrochemical performance measured. In fact, due to special structure of BN which is similar to graphene with small voids, it can act as a bridge for small species when deposited as an ultrathin film [54].

Given the high amount of Vulcan (carbon black of nanoscale domains [55]) in the Pd/C material, its contribution to the kinetics of the studied one electron-transfer process ($Fe(CN)_6^{3-} + e^- = Fe(CN)_6^{4-}$) cannot be completely ruled out. So, we have decided to next interrogate the electrocatalytic abilities towards reactions in potential windows where this contribution is much negligible.

### 3.3. Electrocatalytic performance towards ORR

In order to clarify the actual electrocatalytic trend observed experimentally by the quasi-reversible redox probe molecule, we further considered ORR in 0.1 M NaOH (Fig. 4a) and 0.1 M KOH (Fig. 4b). The voltammograms clearly show that CP-BN-Pd has superior electrochemical performance than other tested catalysts of CP-Pd and Pd/C. Specifically; the results reveal that, on all electrodes, ORR starts at ca. 1 V vs RHE, ultimately approaching the theoretical equilibrium potential of 1.18 V vs RHE. The observed positive shift of 60 mV (0.1 M NaOH) and 25 mV (0.1 M KOH) at CP-BN-Pd electrocatalyst in comparison to CP-Pd at $j$ = 3 mA $cm^{-2}$ can be translated to as an optimal balance between the available active sites for hydroxyl species (the main ORR performance descriptors in alkaline electrolytes [2,3,56]) and $O_2$ species. Given the configuration of the present materials (free-standing), it is not possible to use an (R)RDE and extract the "pure kinetic current". So we use the Tafel plot with the "mass activity" (A per mg of Pd) as reported in Fig. 4c. At 0.9 V vs RHE, the CP-BN-Pd shows a drastic activity increase of one and two order of magnitude compared to the material without BN and the commercial, respectively. Specifically,

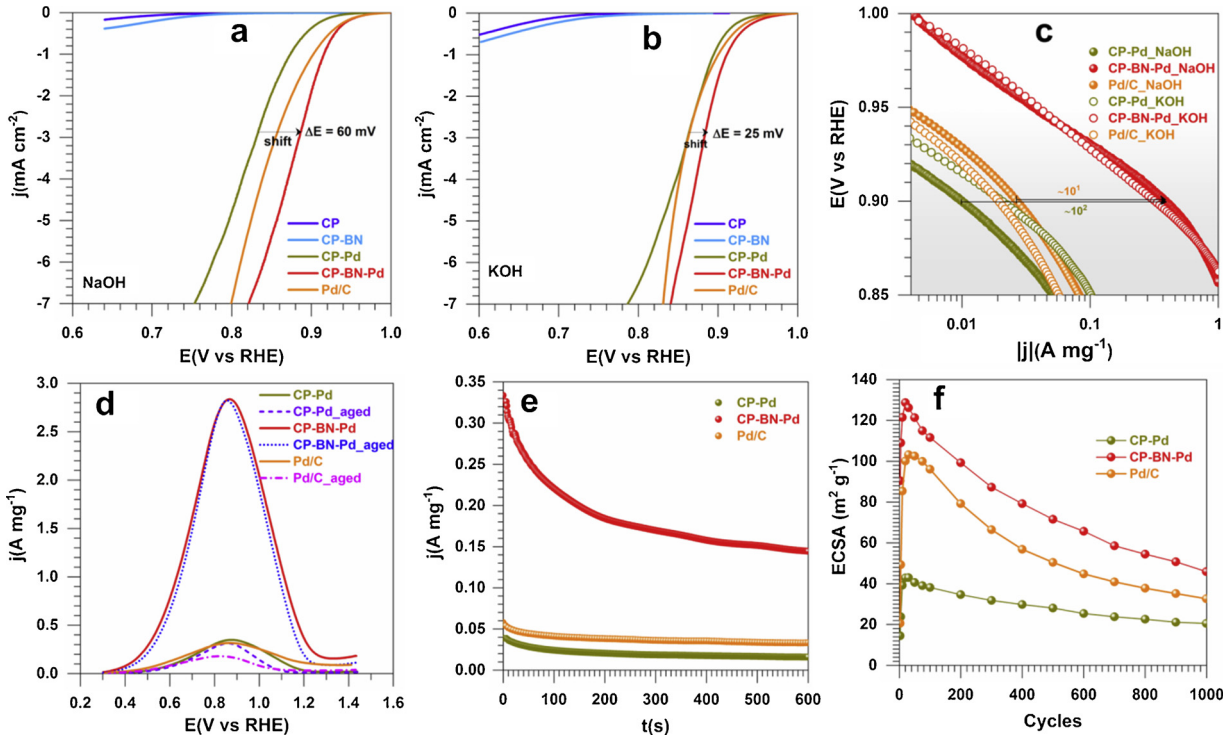


**Fig. 4.** (a) iR-free ORR LSVs recorded in $O_2$-saturated 0.1 M NaOH at 5 mV $s^{-1}$. (b) iR-free ORR LSV recorded in $O_2$-saturated 0.1 M KOH at 5 mV $s^{-1}$. (c) Tafel plots from panels (a) and (b). (d) iR-free steady-state forward CVs recorded at 50 mV $s^{-1}$ in the presence of 0.1 M EtOH before (solid lines) and after (dotted and dashed lines) the accelerated ageing. (e) Chronoamperometry in the presence of 0.1 M EtOH at $E_{appl}$ = 0.6 V vs RHE. (f) ECSA of Pd behavior during the accelerated ageing. The temperature is 25 °C.

a rational comparison with the majority of the literature is not feasible because of the configuration of the present GDL-based materials (free-standing) such as those systems reported in ref. [57]. In fact, it is not possible to use an (R)RDE and extract the "pure kinetic current". So, the most useful method is a direct comparison with Pd/C of about 5 nm as Pd NPs size (the benchmark in alkaline media for ORR) loaded on the same pristine CP. Figs. 4a-4c show that CP-BN-Pd has very high efficiency compared to the tested commercial Pd/C catalyst in both type of alkaline electrolytes. In addition, a tentative comparison with the efficiency of other Pd-based electrocatalysts gathered in ref. [9] clearly indicates that CP-BN-Pd has superior electrochemical performance than the literature in terms of onset potential and kinetics. Overall, the outcomes highlights that CP-BN-Pd aspires to be a potential active cathodic electrocatalyst for ORR in either FCs or metal-air batteries. We further used the technique of EIS to interrogate ORR at the ALD-synthesized samples, firstly at OCP, and secondly at 0.87 V vs RHE in both alkaline electrolytes. As shown in Fig. S8, the complex-plane Nyquist impedance plots recorded in $O_2$-saturated 0.1 M KOH at OCP can be fitted by an EEC of $R_\Omega + Q_{CPE}//R_{ct}$ to extract the data. From the collected data in 0.1 M KOH (Table S4), $R_{ct}$ = 2761 and 33 Ω $cm^2$ for CP-Pd at OCP and 0.87 V vs RHE, respectively. For CP-BN-Pd, the values are 1416 and 28 Ω $cm^2$. The same trend was observed in NaOH electrolyte. These results demonstrate that at OCP where the reaction needs much driving force, the presence of BN nanolayer permits to lower by a factor of nearly two, the energy input to activate $O_2$ molecules at the catalytic surface. Since $R_{ct}$ is correlated to the number of electrons that are transferred from the catalytic surface to the reactant(s) as well as intermediate(s) formation inside the double layer, it can be argued that the presence of BN creates an interface that modifies the electronic properties of Pd and/or C to weaken the substrate binding and regulate the accumulation of intermediates.

### 3.4. Electrocatalytic performance toward C2 alcohols electrooxidation reaction

The previous outcomes demonstrate that we were able to manipulate the ALD synthesis towards electrodes with different electrocatalytic profiles. Except the use of Pd/C commercial material considered to as the benchmark catalyst in alkaline electrolytes [1,4,58], no rational comparison with the literature is feasible for ORR given the configuration of our electrodes. So, we next aimed to study and compared with the literature the newly described materials as electrode materials. For that, we investigated the electrocatalytic properties by considering two model anode reactions in alkaline media that are ethanol and ethylene glycol oxidation. Since stability is an important parameter to be considered when designing catalysts, we also set an electrochemical accelerated ageing program for a dual examination of the ability of the catalysts in maintaining significant ECSA and activity under practical operations. The program consists of cycling the electrode potential from 0.3 to 1.45 V vs RHE (forwards and backward) at 50 mV $s^{-1}$ for a total of 1000 cycles in 0.1 M NaOH (roughly 13 h of continuous operation). The lower potential limit has been fixed to 0.30 V vs RHE to suppress the irreversible insertion of hydrogen in the Pd crystal lattice while the higher potential limit has been set to 1.45 V vs RHE to avoid the formation of superior oxide of $PdO_2$ thus keeping the monolayer charge at 424 μC $cm^{-2}$ [36,59–61]. The electrochemical performance is shown in Fig. 4d-4f in terms of CVs, CA and ECSA. Typical full CVs in the absence or presence of EtOH as well as the recorded voltammograms without current normalization are reported in Fig. S9 while extended CA, CVs at different concentrations of EtOH or scan rate, and ageing CVs are shown within Fig. S10-S14. During the positive-direction scan in the blank electrolyte, the palladium surface oxidation starts at about 0.5 V vs RHE followed by the reduction of the formed PdO during the backward scan at 0.6 V vs RHE on the as-synthesized CP-Pd and CP-BN-Pd catalysts and 0.6-0.5 V vs RHE at Pd/C. From Fig. 4, Table 1 for current density and Fig. S9b for current, one

**Table 1**
Performance of EtOH and EG alcohols electrooxidation from CVs at 50 mV $s^{-1}$.

| Current density $j_p$(A per mg of Pd) | | CP-Pd | CP-BN-Pd | Pd/C |
|---|---|---|---|---|
| 0.1 M NaOH + 0.1 M EtOH | before ageing | 0.35 | 2.84 | 0.32 |
| | after ageing | 0.31 | 2.82 | 0.18 |
| 1 M NaOH + 1 M EtOH | | – | 16.73 | – |
| 0.1 M NaOH + 0.1 M EG | | 0.38 | 3.39 | – |

can see that CP-BN-Pd is undoubtedly the best performing catalyst with excellent stability. Specifically, in the presence of BN, the activity at the peak current displays a negligible decay of 1% while the sample without BN has a significant decay of 11% and commercial Pd/C a prominent activity decay of 44%. Looking deeply at the available ECSA, the values in the beginning of the ageing are 14, 90 and 21 $m^2 g^{-1}$ for CP-Pd, CP-BN-Pd and Pd/C, respectively. The measured activity towards EtOH referred to as "before ageing" was recorded after 20 cycles of surface pre-treatment in electrolyte, corresponding to ECSA of 43, 129 and 100 $m^2 g^{-1}$ for the same trend. Those values become 21, 46 and 33 $m^2 g^{-1}$ at 1000$^{th}$ cycle. The increase of ECSA during the first 30$^{th}$ cycles is rationally assigned to the traditional surface rearrangement phenomenon upon the application of an electrical field between the working and the counter electrodes through the electrode potential.

The achieved ECSA of 90 $m^2 g^{-1}$ at the 3$^{th}$ cycle or 129 $m^2 g^{-1}$ at 20$^{th}$ cycle clearly outperforms the previous reports of ALD-synthesized Pd onto carbon felt electrode [23] and more importantly, those of (electro)chemically-synthesized NPs or self-supported Pd-based electrocatalysts wherein ECSA is about 10-70 $m^2 g^{-1}$, approaching 100 $m^2 g^{-1}$ in bimetallic structures [1,21,22,36,58,62–75]. The high values measured for ECSA in the presence of BN can be assigned to the high dispersion of Pd NPs on the electrode surface (previously shown by TEM) and to the absence of any organic surfactants on the surface of the nanocatalysts as it happens in conventional synthesis by colloidal procedures. The recorded peak current density ($j_p$) of 17 A $mg^{-1}$ (~84 mA $cm^{-2}$) in 1 M NaOH + 1 M EtOH is about 2–10 times higher than relevant reports [10,21,22,68,70–72,74–78] of ethanol electrocatalysis at noble metals mono and bimetallic based on Pd, Au and Pt which are known to provide best up to date values in both alkaline/acidic media (Table S5). In addition to the above literature references and Table S5 that gather relevant data from literature, the use of a commercial Pd/C seems to be one of the best ways to have a good comparison. It can be observed that ALD process enables reinforcing the electrocatalyst stability since after the accelerated ageing, $j_p$ becomes 0.35 and 0.18 A $mg^{-1}$ for CP-Pd (-11%) and Pd/C (-44%), respectively while they had the similar initial performance. Importantly, the presence of "BN bridge" not only enables increasing the initial activity by roughly one order of magnitude, but also keeping this activity during the accelerated ageing (lesser than 1% decrease). We further evaluated the electrocatalytic performance towards ethylene glycol oxidation, another potential candidate for organic molecule-fuelled devices to produce electricity or $H_2$. The peak current densities are gathered in Table 1 while CVs and CA curves are reported in Fig. S15. The value of $j_p$ is 0.38 and 3.39 A $mg^{-1}$ in 0.1 M EG for CP-Pd and CP-BN-Pd, *i.e.*, about 9-times increase of performance; thus underpinning the higher electrochemical activity induced by BN intercalation between carbon surface and Pd NPs. It is anticipated that at higher EG concentration, CP-BN-Pd should largely outperform world-class nanoparticles electrocatalysts, $j_p$ of 3–6 A $mg^{-1}$ in 0.5 M KOH + 0.5 M EG, [65,66] and 0.1–2 A $mg^{-1}$ under other conditions [79–84].

The origin of the present exceptional activity results from several parameters of structural, geometric and electronic order that are well-established in heterogeneous electrocatalysis [15]. Specifically, our

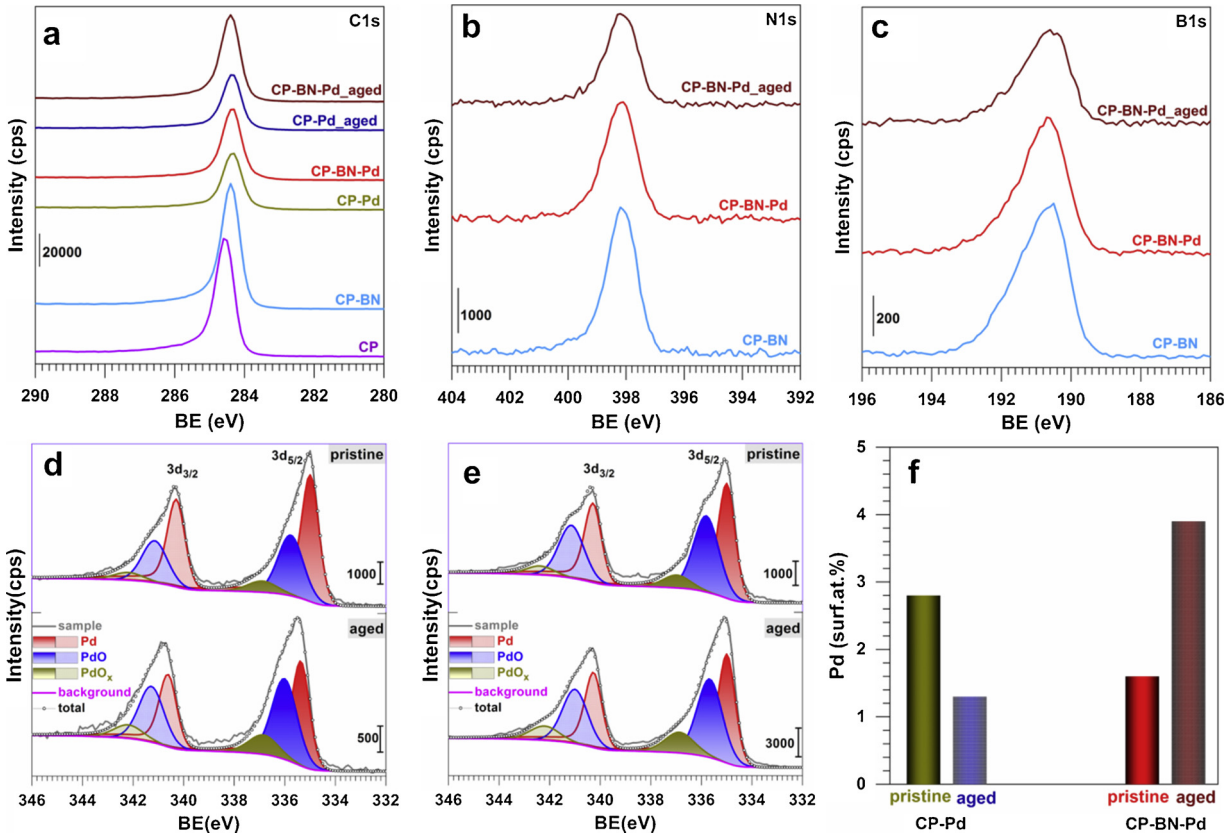


**Fig. 5.** (a–c) High-resolution XPS spectra of the C1s (a), N1s (b), and B1s (c) core levels for the different materials. (d–e) High-resolution XPS spectra of Pd 3d core level before (top) and after (bottom) the accelerated ageing for the as-fabricated CP-Pd and CP-BN-Pd electrode materials, respectively. (f) Quantitative data from the high-resolution XPS measurements of Pd 3d core level of the freshly synthesized (pristine) and after the accelerated ageing program (aged).

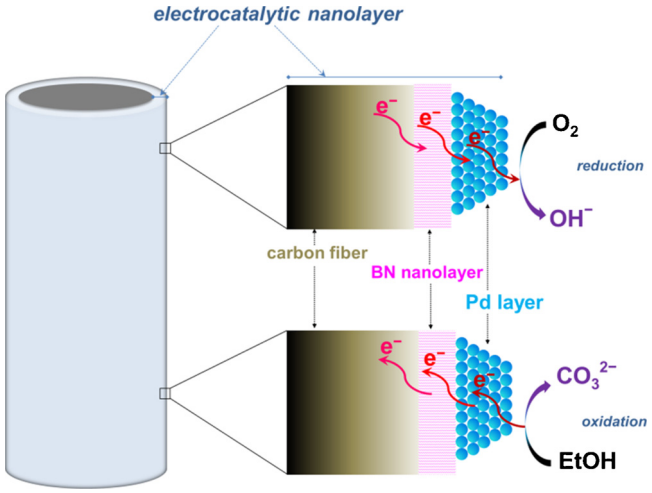


**Scheme 1.** Proposed reaction sketch of the electrocatalysis mechanisms taking place in CP-BN-Pd electrode (left side) during electro-reduction reaction, $O_2$, (right side, top) and electro-oxidation reaction, EtOH, (right side, bottom).

catalysts were obtained in the configuration of simple deposition of Pd NPs on carbon-based substrate, while in most previous studies, NPs are dispersed inside a porous matrix of Vulcan carbon powder to maximize the surface area of the NP catalysts and improve the electron-transfer process. This is followed by further steps of mixing with organic solvents and Nafion suspension as a binder to insure a strong attachment of catalytic species to the surface. So, we believe that the simplicity of the developed approach herein leads to bare uncontaminated surface of nanomaterials in contrast to conventionally-synthesized ones where the surface is blocked by organic byproducts coming from the precursor's decomposition to form NPs. The second reason that might explain the improvement is related to the strong interaction between Pd NPs and the carbon support whose electronic properties have been modified upon the deposition of BN atomic layers.

### *3.5. Compositional and surface characterizations of the as-grown Pd NPs onto CP and CP-BN electrodes*

Having demonstrated the ability to use jointly ALD of BN and Pd to fabricate electrodes with high electrocatalytic properties, we sought to study the surface composition and morphology more carefully. To this end, we employed the surface technique of XPS. Fig. 5 shows the set of results while extended data from XPS spectra fitting are reported in Tables S6-S7. As shown in Fig. 5a and Fig. S16-S17 (survey spectra), the signal of C1s decreases upon the ALD processes indicating that the surface of each individual fiber is being covered by BN film (2 nm) and Pd clusters. Fig. 5b-c highlight the presence of B1s (BE = 190.7 eV) and N1s (BE = 398.1 eV) whose surface compositions are about 6 and 5 at.% before ageing and 4 and 3 at.% after ageing test. The B/N ratio is quasi-constant meaning that the ageing might not affect the structure of BN nanolayer. For the high-resolution XPS spectra of Pd3d core level of the ALD-synthesized Pd NPs of 5 ± 2 nm (Fig. 5d-e), the comparison with the chemically synthesized Pd/C of similar particles size [55] reveals that Pd NPs at the surface are much less oxidized. The identified species are pure Pd metal, PdO, and $PdO_x$ ($x > 1$) [55,85–87]. It is worth of mentioning that, when a metal is exposed to ambient air, it intuitively undergoes a chemical oxidation process because of the oxygen in air. This leads to the formation of a very thin layer, so-called passivation layer, which protects the bulk metal from deep oxidation process. The observed doublets are related to the spin-orbit splitting ($j = l \pm ½$, quantum number $l = 2$ for $d$ band). The metallic state of Pd 3d region is characterized by the two spin–orbital components $3d_{5/2}$ (335.2 eV) and $3d_{3/2}$ (340.5 eV). The table S7 given in SI shows the extended data from XPS spectra fitting. The measured Pd $3d_{5/2}$ binding energy peak (BE = 335.2 eV) level for Pd is the same before and after ageing and corresponds to the position of metallic palladium, which indicates that the Pd NPs are in the Pd(0) state and are stable in the media. From Fig. 5f, one can see that the surface atomic amount of Pd decreases in CP-Pd while that of CP-BN-Pd increases. Since both B and N amounts have decreased in CP-BN-Pd, it is normal to expect an augmentation of total Pd. Looking closely at the SEM image of CP in Fig. 1a, and based of the fact that XPS probes micro-scale domains, it is highly possible that the analyzed area after ageing domains is composed of the inter-connected regions wherein Pd NPs are much important. This can thus rationally explain the increase of Pd3d signal. The augmentation of Pd at the surface of BN coated fibers after potential cycling can lastly be explained by the presence of trace by-products of ALD process of hexafluoroacetylacetonate and formalin that were still remaining on the surface of Pd NPs so that the first voltammetry cycles act as "cleaning" and further re-organization of Pd NPs into a morphology that exposed much atoms at the surface. This is a common observation in electrochemical science and is in agreement with the profiles of ECSA and ethanol oxidation activity. Furthermore, the slight increase of oxidized Pd species in the CP-BN-Pd material in comparison to the unmodified CP-Pd might be explained by the fact that boron nitride attracts electron from Pd similar to previous report [55]. We finally argue that the presence of BN reinforces the tethering of Pd NPs to the surface which can also explain the loose of activity of Pd NPs or their agglomeration into bigger one, i.e., less surface atoms in the CP-Pd material. Conclusively, those outcomes corroborate the findings from electrochemical characterization and catalytic measurements and consolidate our starting hypothesis that atomic layer of boron nitride brings positive effects on the catalytic activity of Pd NPs.

### *3.6. Mechanistic scheme of electrocatalytic reduction and oxidation processes at CP-BN-Pd nano-interface*

To resume these forays toward the deployment of electrocatalytic electrodes derived from the BN and Pd ALD, we finally combined the outcomes to sketch the process in Scheme 1. Since with a nano-bridge of 20–40 Å, electrons coming from the electrode reach $O_2$ substrate (reduction) and those released by the ethanol befall the electrode (oxidation), it is stipulated that the scaffolding created by B and N heteroatoms at the interstitial region are acting as electron relays. Hence, the BN nanolayer plays the role of "bifunctional interface" that regulates the accumulation of intermediates and exchange of electrons.

## 4. Conclusion

In conclusion, we have presented a versatile ALD approach to grow nanostructured palladium (Pd) directly on carbon fibers of a gas-diffusion electrode (GDL). We have relied heavily on electrochemical technics of cyclic voltammetry (CV), chronoamperometry (CA), electrochemical impedance spectroscopy (EIS) as well as transmission electron microscopy (TEM) and X-ray photoelectron spectroscopy (XPS) to provide viable quantitative parameters. By using boron nitride (BN) nano-bridge, we were able to tightly regulate the electrochemical kinetics of the electrodes by the means of the thickness ($x$). Specifically, the rate constant of the redox probe molecule $Fe(CN)_6^{3-}/Fe(CN)_6^{4-}$ has been found to be $k°(10^{-3}$ cm $s^{-1}) = 1.7$, 2.0, 6.2 and 10 for $x = 0$, 10, 20, and 40 Å, respectively. This enhancement of the kinetics was confirmed by oxygen reduction reaction (ORR) with a charge transfer resistance ($R_{ct}$) of 1733, 680, 587 and 520 Ω $cm^2$ in 0.1 M NaOH at 0.81 V vs RHE for the same trend of $x$.

It was also demonstrated that the presence of 2 nm BN film enables not only to significantly reduce the loading of Pd NPs on carbon paper (CP) electrodes of tunable dimensions but also controlling the dispersion to reach exceptional activity and durability for ORR, ethanol oxidation (EtOH), and ethylene oxidation (EG) reactions. In the start-up stage, electrochemically active surface area (ECSA) of 14, 90 and 21

$m^2 g^{-1}$ for CP-Pd, CP-BN-Pd and Pd/C, respectively, represents 4-times increase compared to the benchmark catalyst. After extended electrochemical ageing tests, it was found that the sample without BN losses 54 at.% of Pd and significant activity decay towards ethanol oxidation which was not the case in the presence of BN. A peak current density of $j_p$ = 0.31, 2.82, 0.18 A $mg^{-1}$ for CP-Pd, CP-BN-Pd and Pd/C indicates a 16-times increase for CP-BN-Pd compared to the commercial material. Importantly, the catalytic efficiencies of this advanced CP-BN-Pd electrode towards EtOH and EG electrocatalysis outperform the produced nanocatalysts in the literature. These outstanding outcomes definitely validate the potential interest of boron nitride in electrocatalysis and open prospects for the use of ALD to elaborate bimetallic NPs with even superior catalytic performance.

## Declarations of interest

None.

## Acknowledgement

The French national research agency (ANR, program MeNiNA – ANR-17-CE09-0049), the COST Action "HERALD" (European cooperation program) and the European Institute of Membranes of Montpellier (Exploratory project COGENFC – PAT-Energy-Axis-2018) are acknowledged for funding. The authors thank Bruno Navarra for technical assistance.

## Appendix A. Supplementary data

Supplementary material related to this article can be found, in the online version, at doi:https://doi.org/10.1016/j.apcatb.2019.117917.

## References

[1] H.A. Miller, F. Vizza, M. Marelli, A. Zadick, L. Dubau, M. Chatenet, S. Geiger, S. Cherevko, H. Doan, R.K. Pavlicek, S. Mukerjee, D.R. Dekel, Highly active nanostructured palladium-ceria electrocatalysts for the hydrogen oxidation reaction in alkaline medium, Nano Energy 33 (2017) 293–305.
[2] V.R. Stamenkovic, D. Strmcnik, P.P. Lopes, N.M. Markovic, Energy and fuels from electrochemical interfaces, Nat. Mater. 16 (2017) 57–69.
[3] Z.W. Seh, J. Kibsgaard, C.F. Dickens, I. Chorkendorff, J.K. Nørskov, T.F. Jaramillo, Combining theory and experiment in electrocatalysis: insights into materials design, Science 355 (2017).
[4] T.J. Omasta, X. Peng, H.A. Miller, F. Vizza, L. Wang, J.R. Varcoe, D.R. Dekel, W.E. Mustain, Beyond 1.0 W $cm^{-2}$ performance without platinum: The beginning of a new era in anion exchange membrane fuel cells, J. Electrochem. Soc. 165 (2018) J3039–J3044.
[5] B.P. Setzler, Z. Zhuang, J.A. Wittkopf, Y. Yan, Activity targets for nanostructured platinum-group-metal-free catalysts in hydroxide exchange membrane fuel cells, Nat. Nanotechnol. 11 (2016) 1020.
[6] M.K. Debe, Electrocatalyst approaches and challenges for automotive fuel cells, Nature 486 (2012) 43–51.
[7] A. Brouzgou, A. Podias, P. Tsiakaras, PEMFCs and AEMFCs directly fed with ethanol: a current status comparative review, J. Appl. Electrochem. 43 (2013) 119–136.
[8] H. Zhang, P.K. Shen, Recent development of polymer electrolyte membranes for fuel cells, Chem. Rev. 112 (2012) 2780–2832.
[9] Y. Holade, K. Servat, S. Tingry, T.W. Napporn, H. Remita, D. Cornu, K.B. Kokoh, Advances in electrocatalysis for energy conversion and synthesis of organic molecules, ChemPhysChem 18 (2017) 2573–2605.
[10] L.A. Soares, C. Morais, T.W. Napporn, K.B. Kokoh, P. Olivi, Beneficial effects of rhodium and tin oxide on carbon supported platinum catalysts for ethanol electrooxidation, J. Power Sources 315 (2016) 47–55.
[11] C. Lamy, T. Jaubert, S. Baranton, C. Coutanceau, Clean hydrogen generation through the electrocatalytic oxidation of ethanol in a Proton Exchange Membrane Electrolysis Cell (PEMEC): effect of the nature and structure of the catalytic anode, J. Power Sources 245 (2014) 927–936.
[12] C. Coutanceau, S. Baranton, Electrochemical conversion of alcohols for hydrogen production: a short overview, Wiley Interdiscip. Rev.: Energy Environ. 5 (2016) 388–400.
[13] H.A. Gasteiger, S.S. Kocha, B. Sompalli, F.T. Wagner, Activity benchmarks and requirements for Pt, Pt-alloy, and non-Pt oxygen reduction catalysts for PEMFCs, Appl. Catal. B: Env. 56 (2005) 9–35.
[14] H. Mistry, A.S. Varela, S. Kühl, P. Strasser, B.R. Cuenya, Nanostructured electrocatalysts with tunable activity and selectivity, Nat. Rev. Mater. 1 (2016) 16009.
[15] A.S. Bandarenka, M.T.M. Koper, Structural and electronic effects in heterogeneous electrocatalysis: toward a rational design of electrocatalysts, J. Catal. 308 (2013) 11–24.
[16] E.A. Monyoncho, T.K. Woo, E.A. Baranova, Ethanol electrooxidation reaction in alkaline media for direct ethanol fuel cells, Electrochemistry: Volume 15, The Royal Society of Chemistry, 2019, pp. 1–57.
[17] V. Hacker, S. Mitsushima, Fuel Cells and Hydrogen: From Fundamentals to Applied Research, Elsevier, 2018.
[18] D. Higgins, C. Hahn, C. Xiang, T.F. Jaramillo, A.Z. Weber, Gas-diffusion electrodes for carbon dioxide reduction: a new paradigm, ACS Energy Lett. 4 (2018) 317–324.
[19] N. Cheng, Y. Shao, J. Liu, X. Sun, Electrocatalysts by atomic layer deposition for fuel cell applications, Nano Energy 29 (2016) 220–242.
[20] S.M. George, Atomic layer deposition: an overview, Chem. Rev. 110 (2010) 111–131.
[21] L. Assaud, N. Brazeau, M.K.S. Barr, M. Hanbucken, S. Ntais, E.A. Baranova, L. Santinacci, Atomic layer deposition of Pd Nanoparticles on $TiO_2$ nanotubes for ethanol electrooxidation: synthesis and electrochemical properties, ACS Appl. Mater. Interfaces 7 (2015) 24533–24542.
[22] M.K.S. Barr, L. Assaud, N. Brazeau, M. Hanbücken, S. Ntais, L. Santinacci, E.A. Baranova, Enhancement of Pd catalytic activity toward ethanol electrooxidation by atomic layer deposition of $SnO_2$ onto $TiO_2$ nanotubes, J. Phys. Chem. C 121 (2017) 17727–17736.
[23] M. Weber, P. Collot, H. El Gaddari, S. Tingry, M. Bechelany, Y. Holade, Enhanced catalytic glycerol oxidation activity enabled by activated-carbon-supported palladium catalysts prepared through atomic layer deposition, ChemElectroChem 5 (2018) 743–747.
[24] M. Weber, C. Lamboux, B. Navarra, P. Miele, S. Zanna, M. Dufond, L. Santinacci, M. Bechelany, Boron nitride as a novel support for highly stable palladium nanocatalysts by atomic layer deposition, Nanomaterials 8 (2018) 849.
[25] M.J. Weber, M.A. Verheijen, A.A. Bol, W.M.M. Kessels, Sub-nanometer dimensions control of core/shell nanoparticles prepared by atomic layer deposition, Nanotechnology 26 (2015) 094002.
[26] A.J.M. Mackus, M.J. Weber, N.F.W. Thissen, D. Garcia-Alonso, R.H.J. Vervuurt, S. Assali, A.A. Bol, M.A. Verheijen, W.M.M. Kessels, Atomic layer deposition of Pd and Pt nanoparticles for catalysis: on the mechanisms of nanoparticle formation, Nanotechnology 27 (2015) 034001.
[27] F. Zaera, The surface chemistry of thin film atomic layer deposition (ALD) processes for electronic device manufacturing, J. Mater. Chem. 18 (2008) 3521–3526.
[28] S. Chen, Z. Chen, S. Siahrostami, D. Higgins, D. Nordlund, D. Sokaras, T.R. Kim, Y. Liu, X. Yan, E. Nilsson, R. Sinclair, J.K. Nørskov, T.F. Jaramillo, Z. Bao, Designing boron nitride islands in carbon materials for efficient electrochemical synthesis of hydrogen peroxide, J. Am. Chem. Soc. 140 (2018) 7851–7859.
[29] M. Weber, J.-H. Kim, J.-H. Lee, J.-Y. Kim, I. Iatsunskyi, E. Coy, M. Drobek, A. Julbe, M. Bechelany, S.S. Kim, High-performance nanowire hydrogen sensors by exploiting the synergistic effect of Pd Nanoparticles and metal–organic framework membranes, ACS Appl. Mater. Interfaces 10 (2018) 34765–34773.
[30] Y. Liu, Y. Zhang, K. Cheng, X. Quan, X. Fan, Y. Su, S. Chen, H. Zhao, Y. Zhang, H. Yu, M.R. Hoffmann, Selective electrochemical reduction of carbon dioxide to ethanol on a boron- and nitrogen-co-doped nanodiamond, Angew. Chem. Int. Ed. 56 (2017) 15607–15611.
[31] M. Chhetri, S. Maitra, H. Chakraborty, U.V. Waghmare, C.N.R. Rao, Superior performance of borocarbonitrides, BxCyNz, as stable, low-cost metal-free electrocatalysts for the hydrogen evolution reaction, Energy Environ. Sci. 9 (2016) 95–101.
[32] C. Huang, C. Chen, M. Zhang, L. Lin, X. Ye, S. Lin, M. Antonietti, X. Wang, Carbon-doped BN nanosheets for metal-free photoredox catalysis, Nat. Commun. 6 (2015) 7698.
[33] B. Boekfa, P. Treesukol, Y. Injongkol, T. Maihom, P. Maitarad, J. Limtrakul, The Activation of Methane on Ru, Rh, and Pd decorated carbon nanotube and boron nitride nanotube: a DFT Study, Catalysts 8 (2018) 190.
[34] Q. Sun, C. Sun, A. Du, S. Dou, Z. Li, In-plane graphene/boron-nitride heterostructures as an efficient metal-free electrocatalyst for the oxygen reduction reaction, Nanoscale 8 (2016) 14084–14091.
[35] M. Weber, B. Koonkaew, S. Balme, I. Utke, F. Picaud, I. Iatsunskyi, E. Coy, P. Miele, M. Bechelany, Boron nitride nanoporous membranes with high surface charge by atomic layer deposition, ACS Appl. Mater. Interfaces 9 (2017) 16669–16678.
[36] Y. Holade, C. Morais, K. Servat, T.W. Napporn, K.B. Kokoh, Toward the Electrochemical Valorization of Glycerol: fourier transform infrared spectroscopic and chromatographic studies, ACS Catal. 3 (2013) 2403–2411.
[37] M. Grdeń, M. Lukaszewski, G. Jerkiewicz, A. Czerwinski, Electrochemical behaviour of palladium electrode: oxidation, electrodissolution and ionic adsorption, Electrochim. Acta 53 (2008) 7583–7598.
[38] B. Mårlid, M. Ottosson, U. Pettersson, K. Larsson, J.-O. Carlsson, Atomic layer deposition of BN thin films, Thin Solid Films 402 (2002) 167–171.
[39] J. Heinze, Cyclic voltammetry – "Electrochemical spectroscopy". New analytical methods (25), Angew. Chem. Int. Ed. 23 (1984) 831–847.
[40] E. Mahé, D. Devilliers, C. Comninellis, Electrochemical reactivity at graphitic microdomains on polycrystalline boron doped diamond thin-films electrodes, Electrochim. Acta 50 (2005) 2263–2277.
[41] A.L. Eckermann, D.J. Feld, J.A. Shaw, T.J. Meade, Electrochemistry of redox-active self-assembled monolayers, Coord. Chem. Rev. 254 (2010) 1769–1802.
[42] R.S. Nicholson, Theory and application of cyclic voltammetry for measurement of electrode reaction kinetics, Anal. Chem. 37 (1965) 1351–1355.
[43] A. Lasia, Electrochemical Impedance Spectroscopy and Its Applications, Springer-Verlag, New York, NY, USA, 2014.
[44] M.E. Orazem, B. Tribollet, Electrochemical Impedance Spectroscopy, 2 ed., John

Wiley & Sons, Inc., Hoboken, New Jersey, USA, 2017.
[45] A.J. Bard, L.R. Faulkner, Electrochemical Methods: Fundamentals and Applications, 2nd ed., John Wiley & Sons, Inc., USA, 2001.
[46] N. Tanaka, R. Tamamushi, Kinetic parameters of electrode reactions, Electrochim. Acta 9 (1964) 963–989.
[47] A.M. Bond, Broadening Electrochemical Horizons: Principles and Illustration of Voltammetric and Related Techniques, Oxford University Press Inc., New York, USA, 2002.
[48] W.E. Kosimaningrum, T.X.H. Le, Y. Holade, M. Bechelany, S. Tingry, B. Buchari, I. Noviandri, C. Innocent, M. Cretin, Surfactant- and binder-free hierarchical platinum nanoarrays directly grown onto a carbon felt electrode for efficient electrocatalysis, ACS Appl. Mater. Interfaces 9 (2017) 22476–22489.
[49] Z. Ling, Z. Wang, M. Zhang, C. Yu, G. Wang, Y. Dong, S. Liu, Y. Wang, J. Qiu, Sustainable synthesis and assembly of biomass-derived B/N Co-doped carbon nanosheets with ultrahigh aspect ratio for high-performance supercapacitors, Adv. Funct. Mater. 26 (2016) 111–119.
[50] Z.-S. Wu, A. Winter, L. Chen, Y. Sun, A. Turchanin, X. Feng, K. Müllen, Three-dimensional nitrogen and boron Co-doped graphene for high-performance all-solid-state supercapacitors, Adv. Mater. 24 (2012) 5130–5135.
[51] Z. Liu, L. Ma, G. Shi, W. Zhou, Y. Gong, S. Lei, X. Yang, J. Zhang, J. Yu, K.P. Hackenberg, A. Babakhani, J.-C. Idrobo, R. Vajtai, J. Lou, P.M. Ajayan, In-plane heterostructures of graphene and hexagonal boron nitride with controlled domain sizes, Nat. Nanotechnol. 8 (2013) 119.
[52] J. Olander, K. Larsson, Initial growth of hexagonal and cubic boron nitride: a theoretical study, Phys. Rev. B 68 (2003) 075411.
[53] R. Laskowski, P. Blaha, K. Schwarz, Bonding of hexagonal BN to transition metal surfaces: an ab initio density-functional theory study, Phys. Rev. B 78 (2008) 045409.
[54] C.W. Hamilton, R.T. Baker, A. Staubitz, I. Manners, B-N compounds for chemical hydrogen storage, Chem. Soc. Rev. 38 (2009) 279–293.
[55] Y. Holade, C. Canaff, S. Poulin, T.W. Napporn, K. Servat, K.B. Kokoh, High impact of the reducing agent on palladium nanomaterials: new insights from X-ray photoelectron spectroscopy and oxygen reduction reaction, RSC Adv. 6 (2016) 12627–12637.
[56] K.A. Stoerzinger, M. Risch, B. Han, Y. Shao-Horn, Recent insights into manganese oxides in catalyzing oxygen reduction kinetics, ACS Catal. 5 (2015) 6021–6031.
[57] D.P. Valencia, L. Yate, W. Aperador, Y. Li, E. Coy, High electrocatalytic response of ultra-refractory ternary alloys of Ta-Hf-C carbide toward hydrogen evolution reaction in acidic media, J. Phys. Chem. C 122 (2018) 25433–25440.
[58] H.A. Miller, A. Lavacchi, F. Vizza, M. Marelli, F. Di Benedetto, F. D'Acapito, Y. Paska, M. Page, D.R. Dekel, A Pd/C-$CeO_2$ Anode catalyst for high-performance platinum-free anion exchange membrane fuel cells, Angew. Chem. Int. Ed. 55 (2016) 6004–6007.
[59] A. Zalineeva, S. Baranton, C. Coutanceau, G. Jerkiewicz, Octahedral palladium nanoparticles as excellent hosts for electrochemically adsorbed and absorbed hydrogen, Sci. Adv. 3 (2017).
[60] C.-C. Hu, T.-C. Wen, Voltammetric investigation of palladium oxides − I: their formation/reduction in NaOH, Electrochim. Acta 40 (1995) 495–503.
[61] Y. Wang, Z.M. Sheng, H. Yang, S.P. Jiang, C.M. Li, Electrocatalysis of carbon black- or activated carbon nanotubes-supported Pd-Ag towards methanol oxidation in alkaline media, Int. J. Hydrogen Energy 35 (2010) 10087–10093.
[62] A. Zalineeva, A. Serov, M. Padilla, U. Martinez, K. Artyushkova, S. Baranton, C. Coutanceau, P.B. Atanassov, Self-Supported PdxBi catalysts for the electrooxidation of glycerol in alkaline media, J. Am. Chem. Soc. 136 (2014) 3937–3945.
[63] A. Serov, U. Martinez, P. Atanassov, Novel Pd-In catalysts for alcohols electrooxidation in alkaline media, Electrochem. commun. 34 (2013) 185–188.
[64] M. Simões, S. Baranton, C. Coutanceau, Electro-oxidation of glycerol at Pd based nano-catalysts for an application in alkaline fuel cells for chemicals and energy cogeneration, Appl. Catal. B: Env. 93 (2010) 354–362.
[65] W. Hong, C. Shang, J. Wang, E. Wang, Bimetallic PdPt nanowire networks with enhanced electrocatalytic activity for ethylene glycol and glycerol oxidation, Energy Environ. Sci. 8 (2015) 2910–2915.
[66] S. Li, J. Lai, R. Luque, G. Xu, Designed multimetallic Pd nanosponges with enhanced electrocatalytic activity for ethylene glycol and glycerol oxidation, Energy Environ. Sci. 9 (2016) 3097–3102.
[67] L.M. Palma, T.S. Almeida, C. Morais, T.W. Napporn, K.B. Kokoh, A.R. de Andrade, Effect of co-catalyst on the selective electrooxidation of glycerol over ruthenium-based nanomaterials, ChemElectroChem 4 (2017) 39–45.
[68] S. Ghosh, S. Bera, S. Bysakh, R.N. Basu, Highly active multimetallic palladium nanoalloys embedded in conducting polymer as anode catalyst for electrooxidation of ethanol, ACS Appl. Mater. Interfaces 9 (2017) 33775–33790.
[69] S. Ghosh, A.-L. Teillout, D. Floresyona, P. de Oliveira, A. Hagège, H. Remita, Conducting polymer-supported palladium nanoplates for applications in direct alcohol oxidation, Int. J. Hydrogen Energy 40 (2015) 4951–4959.
[70] S. Ghosh, H. Remita, P. Kar, S. Choudhury, S. Sardar, P. Beaunier, P.S. Roy, S.K. Bhattacharya, S.K. Pal, Facile synthesis of Pd nanostructures in hexagonal mesophases as a promising electrocatalyst for ethanol oxidation, J. Mater. Chem. A Mater. Energy Sustain. 3 (2015) 9517–9527.
[71] F. Ksar, G. Surendran, L. Ramos, B. Keita, L. Nadjo, E. Prouzet, P. Beaunier, A. Hagège, F. Audonnet, H. Remita, Palladium nanowires synthesized in hexagonal mesophases: application in ethanol electrooxidation, Chem. Mater. 21 (2009) 1612–1617.
[72] F. Ksar, L. Ramos, B. Keita, L. Nadjo, P. Beaunier, H. Remita, Bimetallic palladium-gold nanostructures: application in ethanol oxidation, Chem. Mater. 21 (2009) 3677–3683.
[73] C. Zhu, S. Guo, S. Dong, PdM (M = Pt, Au) Bimetallic alloy nanowires with enhanced electrocatalytic activity for electro-oxidation of small molecules, Adv. Mater. 24 (2012) 2326–2331.
[74] T. Miao, Y. Song, C. Bi, H. Xia, D. Wang, X. Tao, Correlation of surface Ag content in AgPd shells of ultrasmall core-shell Au@AgPd nanoparticles with enhanced electrocatalytic performance for ethanol oxidation, J. Phys. Chem. C 119 (2015) 18434–18443.
[75] L.Y. Chen, N. Chen, Y. Hou, Z.C. Wang, S.H. Lv, T. Fujita, J.H. Jiang, A. Hirata, M.W. Chen, Geometrically controlled nanoporous PdAu bimetallic catalysts with tunable Pd/Au ratio for direct ethanol fuel cells, ACS Catal. 3 (2013) 1220–1230.
[76] L.M. Palma, T.S. Almeida, P.H. Leonello, A.R.D. Andrade, Ethanol electrooxidation by plurimetallic Pt-based electrocatalysts prepared by microwave assisted heating, J. Electrochem. Soc. 161 (2014) F473–F479.
[77] V. Bambagioni, C. Bianchini, J. Filippi, W. Oberhauser, A. Marchionni, F. Vizza, R. Psaro, L. Sordelli, M.L. Foresti, M. Innocenti, Ethanol oxidation on electrocatalysts obtained by spontaneous deposition of palladium onto nickel-zinc materials, ChemSusChem 2 (2009) 99–112.
[78] Y.-Y. Feng, Z.-H. Liu, Y. Xu, P. Wang, W.-H. Wang, D.-S. Kong, Highly active PdAu alloy catalysts for ethanol electro-oxidation, J. Power Sources 232 (2013) 99–105.
[79] H. Wang, B. Jiang, T.-T. Zhao, K. Jiang, Y.-Y. Yang, J. Zhang, Z. Xie, W.-B. Cai, Electrocatalysis of Ethylene Glycol Oxidation on Bare and Bi-Modified Pd concave nanocubes in alkaline solution: an interfacial infrared spectroscopic investigation, ACS Catal. 7 (2017) 2033–2041.
[80] J. Qi, N. Benipal, C. Liang, W. Li, PdAg/CNT catalyzed alcohol oxidation reaction for high-performance anion exchange membrane direct alcohol fuel cell (alcohol = methanol, ethanol, ethylene glycol and glycerol), Appl. Catal. B: Env. 199 (2016) 494–503.
[81] Y. Kim, H. Kim, W.B. Kim, PtAg nanotubes for electrooxidation of ethylene glycol and glycerol in alkaline media, Electrochem. commun. 46 (2014) 36–39.
[82] D. González-Quijano, W.J. Pech-Rodríguez, J.I. Escalante-García, G. Vargas-Gutiérrez, F.J. Rodríguez-Varela, Electrocatalysts for ethanol and ethylene glycol oxidation reactions. Part I: effects of the polyol synthesis conditions on the characteristics and catalytic activity of Pt-Sn/C anodes, Int. J. Hydrogen Energy 39 (2014) 16676–16685.
[83] A. Marchionni, M. Bevilacqua, C. Bianchini, Y.-X. Chen, J. Filippi, P. Fornasiero, A. Lavacchi, H. Miller, L. Wang, F. Vizza, Electrooxidation of ethylene glycol and glycerol on Pd-(Ni-Zn)/C anodes in direct alcohol fuel cells, ChemSusChem 6 (2013) 518–528.
[84] Z.Y. Li, Y.J. Liang, S.P. Jiang, X.D. Shan, M.L. Lin, C.W. Xu, Electrooxidation of methanol and ethylene glycol mixture on platinum and palladium in alkaline medium, Fuel Cells Weinh. (Weinh) 12 (2012) 677–682.
[85] K.S. Kim, A.F. Gossmann, N. Winograd, X-ray photoelectron spectroscopic studies of palladium oxides and the palladium-oxygen electrode, Anal. Chem. 46 (1974) 197–200.
[86] L.S. Kibis, A.I. Stadnichenko, S.V. Koscheev, V.I. Zaikovskii, A.I. Boronin, Highly oxidized palladium nanoparticles comprising $Pd^{4+}$ species: spectroscopic and structural aspects, thermal stability, and reactivity, J. Phys. Chem. C 116 (2012) 19342–19348.
[87] L.S. Kibis, A.I. Titkov, A.I. Stadnichenko, S.V. Koscheev, A.I. Boronin, X-ray photoelectron spectroscopy study of Pd oxidation by RF discharge in oxygen, Appl. Surf. Sci. 255 (2009) 9248–9254.